UNE ÉTUDE DE CAS:

EXAMEN DE L'EFFET DE LA PLUIE SUR NEIGE À L'AIDE DES MICRO-ONDES PASSIVES

Par:

Vukasin Todorovic

Essai présenté au Département de géomatique appliquée

en vue d'obtention du grade de maître en sciences (M.Sc)

Sous la direction de Dr. Alexandre Langlois

MAITRISE EN SCIENCES GEOGRAPHIQUES

UNIVERSITÉ DE SHERBROOKE

Décembre 2013

EXAMINING RAIN ON SNOW FROM A PASSIVE MICROWAVE PERSPECTIVE: A CASE STUDY

By

Vukasin Todorovic

An essay submitted to Département de géomatique appliquée

In partial fulfilment of the requirements for the degree of Master of Sciences

Essay Supervisor Dr. Alexandre Langlois

MASTERS IN GEOGRAPHICAL SCIENCES

UNIVERSITÉ DE SHERBROOKE

December 2013

Sommaire

L'Arctique est une des régions de notre planète les plus sensibles au réchauffement climatique. Les effets de pluie sur neige ne sont pas pris en considération dans les modèles climatiques globaux ainsi augmentant leurs incertitudes. La présence de l'eau dans une colonne de neige a un impact direct sur l'albédo ainsi que sur les propriétés diélectriques de la neige. Même si ces effets ont un impact direct sur les propriétés de la neige, ce qui contribue d'une manière positive au réchauffement climatique, il n'existe pas une méthode empirique de détection de ce phénomène. Des recherches précédentes sur ce sujet on démontrée que les fréquences de 19 et 37 GHz dans les micro-ondes passives sont d'une grande sensibilité a la présence de l'eau dans la neige. Cet essai propose, analyse et réalise un test validation d'une méthode qui met en relation les polarisations verticales et horizontales des fréquences mentionnées précédemment ($GR_P = \frac{GRV}{GRH}$) pour les fins de détection de phénomène de pluie sur neige.

La présence de l'eau dans une colonne de neige va augmenter la température de brillance dans le 19V, 37H et 37H, mais pas pour le 19H. La température de brillance de ce dernier va diminuer. En créant un ratio de gradient entre les deux polarisations ($GR_P = \frac{GRV}{GRH}$) le phénomène de pluie sur neige va provoquer des valeurs négatives de ce dernier, tandis que les valeurs positives indiqueront des circonstances météorologiques normales ou de fonte (non liée à la pluie sur neige). La validation de cette méthode, en utilisant des données d'AMSR-E et des observations météorologique humaines de l'Environnement Canada, indique des résultats prometteurs avec des faibles valeurs d'omission, de commission, et d'inexactitude. Une étude plus poussée permettra de réduire l'inexactitude de l'index proposé et nous permettra d'obtenir une méthode empirique viable pour détecter le phénomène de pluie sur neige.

Abstract

The environmental and anthropocentric forcings have a significant impact on climate change and the rate at which it is happening. Even if the rain on snow (ROS) events are known to be an important part of the previously mentioned forcings, they are not taken into consideration in global climate models given the absence of a yet reliable empiric method for detecting their occurrence. Previous research has shown that the 19 GHz and 37 GHz passive microwave frequencies are highly sensitive to presence of liquid water within the snow column. By examining the normalized gradient (GR) of the polarized components, horizontal (H) and vertical (V), of the previously mentioned frequencies, we have created a ROS detection approach using the gradient ratios between GRV and GRH gradients. The validation of the approach using AMSR-E data over known ROS events (in-situ observed meteorological data) demonstrates the promising potential of the index and suggests that further research into this subject might allow us to create a reliable and operational remote sensing ROS detection method.

Table of contents

Tables

Figures

1.0. Introduction

The climate is constantly changing and that on both micro and macro temporal and spatial scales (White et al., 2010). There is a growing understanding regarding the causes of long-term climate change; variation in incoming solar radiation, ocean circulation patterns, atmospheric circulation patterns as well as many other variables each with their own positive and negative feedback mechanisms (Schrank, 2007; White et al., 2010). Climatic variability that takes hundreds, thousands or even millions of years to occur do not represent a substantial problem from an environmental and/or anthropocentric views; if enough time is given, the environment as well as human societies, can adapt to change (Schrank, 2007; White et al., 2010). However, the short-term climate variability and change will result in the most adaptation problems from the environmental and anthropocentric point of views (White et al., 2010).

International Panel on Climate Change (IPCC) has been forecasting climate change predictions and their potential effects over the past couple of decades. On several of their reports, including the most recent one in 2013, IPCC has confirmed that the Arctic region, from the climate variability point of view, is one of the most sensitive regions on our planet. It is thanks to research into the intricate global network of climate related positive and negative feedbacks converging in the Arctic region that we came to understand that particular region's vulnerability to climate change (Francis et al., 2005). Rising temperatures in the Arctic will result in such events as rain on snow, heat wave, blizzards and many other extreme winter events. It is important to note that the ROS events are not taken into account in the climate models. Furthermore, by not taking into account all the variables, the uncertainty of the global circulation models (GCM's) becomes even higher (Hardiman et al., 2008; Dutra et al., 2010). The uncertainty becomes even greater if we take into consideration the lack of the in-situ meteorological measurements for the Arctic Circle region.

From a global point of view, eight countries border the Arctic: Russia, United States, Canada, Denmark, Finland, Norway, Iceland and Sweden. With the recent increase in the global energy consumption, all eight countries have very strong socioeconomic interests in the Arctic region, resulting in an increase in the local exploration and

exploitation. It is undeniable that the changes highlighted above can also have some positive socioeconomic benefits. Arctic continental shelves are believed to be one of the richest in carbon fuels on the planet (Read and Lermit, 2005). Until now, exploitation of those resources has been heavily deterred by Arctic harsh climatic conditions and sea ice (the access), but the current sea ice retreat and snow melt suggest that such activities would become viable. Hence, understanding the impact of ROS and other extreme events on the surface conditions in the northern regions is critical for natives, traditional resource users, scientists and other stakeholders in order to develop mitigative responses and adaptive strategies in this changing environment. Sadly, even just the prospect of such possibilities and the potential gains are creating socioeconomic tensions between the Arctic Circle nations.

As it is implied in the title, the following essay will present a case study of the effects of rain on snow events from a passive microwave perspective. Specifically, this essay aims at improving our empirical understanding on the effect of ROS on snow properties and associated passive microwave response. This will allow the analysis on the 'detectability' of such events from space that could potentially yield temporal and spatial trends in event occurrence. Specifically, this study aims at;

a) Provide brightness temperatures behaviours at 19 and 37 GHz under melting snow condition and ROS events.
b) Evaluate brightness temperature indexes (polarization ratio, gradient ratio) during both melt and ROS events
c) Investigate the development of an empirical ROS detection algorithm and evaluate its application from space.

In order to understand the principles involved behind such a study and its importance, the current essay is structured with a background section (climate change in the arctic, importance of snow, warming and rain on snow (ROS), remote sensing and impact of rain on snow will be discussed) before outlining, the methodology, the study area, the results, the validation, discussion of limitations and the conclusion.

2.0. Background

2.1. Climate change in the Arctic

Arctic appears to be the most climate change sensitive region on our planet (ACIA, 2004; Kattsov and Kallen, 2005, Ford et al., 2006). Mean annual temperatures have seen an increase of 2°C in the last 60 years while Arctic's winter mean seasonal temperatures have seen an increase of 4°C (ACIA. 2004). As a direct consequence to warming temperatures, changes in precipitation regime (amount and phase), extensive melting of permafrost, retreat of Arctic glaciers, sea ice thickness and extent reduction and snow cover duration decline (Brown and Mote 2008; Derksen and Brown, 2013) have been observed over the past four decades (IPCC, 2013).

The consequences of such dramatic climatic change has been widely debated (IPCC, 2013). It is believed that a reduction of snow cover extent and duration could ultimately impact the permafrost growth and inevitably result in its melting. This would result in a release of enormous quantities of methane gas, produced by organic decomposition and entrapped below the permafrost layer, thus contributing to a positive feedback effect of climate change (Romanovsky et al., 2010). Furthermore, the rise of global sea level due to on land ice and glacier melt from the arctic also has some scientists and coastal communities worried given the substantial amounts of land ice in Artic regions (Rahmstorf, 2007). Because snow and ice have a higher albedo than bare soil, water and/or vegetation, higher amounts of incoming solar radiation are being reflected directly back into space and thus do not contribute toward the surface warming. Hence, with the reduction of snow cover extent and duration, combined with the reduction in sea ice extent and thickness, more energy can be absorbed by the underlying layers for which the albedo is smaller and thus contributing more to the melting through a positive feedback cycle.

2.2. Modeling Challenges

Climate prediction forecasts are only as good as the models and the data provided as inputs. There are still large uncertainties in regards to the effects of snow on climatologically heating and cooling patterns (Fletcher et al. 2009). Global circulation

models (GCMs), use input information plagued with certain amounts of uncertainty, which in return produce inaccurate climate predictions (Brown et al., 2003 Langlois et al., 2013). These uncertainties become substantial when dealing with northern latitudes where the observed warming is the strongest simply because there is a bias and/or lack of data (Kaufman et al, 2009). Because of the inaccessibility of the northern latitudes, harsh weather conditions and the lack of human settlements and high research and data gathering costs, data gathering bias can be created simply because it becomes easier to collect data in southern regions. These settlements are often found in the coastal areas which might not represent the general climatic trends of the wider region.

Data availability for validations has been pointed out as one of the main bottlenecks throughout many researches. In order to surmount this challenge, scientists have kept increasing the spatial and temporal resolutions of remote sensing products to augment the overlap between the observed data and the available in situ measurements. Of particular relevance, passive microwaves are correlated to snow thermophysical properties, but the effects of ROS on the emissions require more understanding. Because of their relative indifference to weather conditions, darkness, as well as their sensitivity to changes in the snow properties, passive microwaves are considered to be one of the best ways to study snow-covered surfaces by the means of satellite remote sensing (Ulaby et al, 1986). But, the passive microwave approach is not without its challenges (Kelly et al., 2003; Langlois et al., 2010); large spatial resolution often results in encompassing a wide range of different surfaces within one and same pixel each of which contributing in their own way to the signal, ultimately affecting the signal interpretation (Makynen and Hallikainen, 2005; Langlois et al., 2011; Roy et al., 2012). In order to surmount those challenges, the problem must be approached from multiple scales (such as proposed herein) and in-situ validation of the satellite measurements often presents itself as one of the best solutions. Never the less, the initial problem mentioned at the beginning of this paragraph still persists; the remote sensing method does not yet offer a rain on snow phenomenon retrieval method.

2.3. Surface Energy Balance

One of the main effects of ROS is the changes on the surface energy balance (SEB). Changes under such circumstances, associated with the fact that the Arctic plays an important role in the global energy balance equation, can be significant. The SEB is largely controlled by the radiation and turbulent fluxes balance. The radiation balance can be simply defined as the difference between the incoming solar (K↓) and longwave (L↓) radiation and the emitted longwave (L↑) and reflected solar radiation (K↑). The difference between the two is the amount of energy that is at the surface thus contributes toward the warming of the climate and the surface melt.

$$Q = K\downarrow - K\uparrow + L\downarrow - L\uparrow + Q_h + Q_e + Q_c + Q_p \quad \text{[eq. 1]}$$

$$\text{Albedo} = K\uparrow / K\downarrow$$

Q = Energy balance

K = Short wave radiation

L = Long wave radiation

Q_h = Sensible heat flux

Q_e = Latent heat flux

Q_c = Conductive flux

Q_p = Heat conducted by precipitation

↓ = Incoming

↑ = Outgoing

The last portion of the energy balance equation, ($Q_h + Q_e + Q_c + Q_p$), is also referred to as turbulent fluxes. Latent heat flux (Q_e), is associated with phase change; evaporation and sublimation both result in entrapment of latent heat, while condensation results in the release of that latent heat. Sensible heat flux (Q_h) is not necessarily associated with the phase change. It happens simply between two surfaces where temperature difference exists where the energy will flow from the relatively hotter surface toward the relatively cooler surface until the equilibrium is reached. The turbulent fluxes are related to atmospheric stability where an increase in atmospheric stability translates into a reduction of turbulent fluxes and a decrease of atmospheric stability results into an increase of turbulent fluxes. For instance, a warm front associated with ROS will lead to a decrease in atmospheric stability due to its characteristics such as increasing

temperature, wind speed and relative humidity causing an increased sensible heat flux towards the surface. A negative sensible heat flux from the surface toward the atmosphere can occur after low-pressure system passing or during a cold front. In both cases, sensible heat flux toward the atmosphere, referred to as negative sensible heat flux, can only happen during atmospheric temperatures below 0°C, while positive sensible heat fluxes can occur both above and below 0°C (Steffen and DeMaria, 1996)

2.4. Precipitations

Precipitations can only occur once saturation conditions are met. Because temperature decreases with the increasing altitude, the process of buoyancy that lifts a heated mass of air will inevitably also cause it to cool down. Once the dew point is reached, the condensation will occur. It is outside the scope of this essay to go into all possible condensation methods, but suffice to say that the condensation will happen around condensation nuclei, a small particulate like a speck of dust, sand, ice, or even bacteria. The water droplet will then grow through coalescence and gain enough mass to overcome convection and surrender to the laws of gravity.

Similarly to rain, snow is formed through the same process in its beginning. In order for water droplets to become snow, sub-zero temperatures are required as well as nucleating agent which becomes active below -4°C. In the atmosphere, water droplets do not freeze at 0°C. This phenomenon leads to the creation of supercooled water droplets. Two nucleation methods, homogenous and heterogeneous, can result in ice crystal formation. Heterogeneous nucleation occurs when vapour deposits on ice nuclei, immersion-freezing, and collision between supercooled droplets and ice nuclei. Homogenous nucleation occurs at temperatures of -40°C when supercooled droplets can spontaneously become ice crystals. It is only once the ice crystal has formed that they can grow and become snowflakes. There are three main mechanisms behind ice crystal growth namely: 1) supersaturation of water vapour over ice; 2) aggregation, which defines the process of collision and adhesion of ice particles; and 3) riming, adhesion of supercooled water onto ice crystals.

Although solid precipitations are expected in winter conditions, rain can still persist as a phenomenon known as rain-on-snow events given the actual warming observed in the Arctic. As such, very little is known about rain on snow events that occur in northern latitudes and their cumulative effects on the surface energy balance. The presence of water in a snow pack can severely affect its energy transfer mechanisms, water having a higher thermal conductivity then snow or air and thus facilitating energy fluxes throughout the snow. Given the fact that the temperatures are rising in the north, it can be expected that the ROS events will rise in frequency. As such, Vincent and Mekis (2006) have shown that, in southern regions, the snow precipitations to total ratio have decrease by 10 to 20% in the last hundred years inferring an increase in liquid precipitation. Other researches have shown a widespread increase in frequency of the number of ROS days in the Arctic region between 1979 and 2009 (Liston and Hiemstra, 2011); Canadian Arctic Archipelago and Baffin Island have seen a steady increase in the number of ROS days in the last decades. ROS have also been shown to impact northern biota since water percolation can reach freezing conditions leading to the formation of ice layers. This process is known to affect grazing conditions of several species (Putkonen and Roe, 2003), which motivated some of the pioneer work in ROS retrieval from space (Grenfell and Putkonen, 2008)

As such, several studies have approached the subject with some degree of success showing correlations between brightness temperatures and snow wetness (Arslan et al., 2001; Grenfell and Putkonen, 2008). However, the lack of in-situ data persists as the main reason for a lack in understanding and precise retrievals of ROS events by means of remote sensing. Furthermore, detection algorithms have yet to be developed in order to analyze trends in event occurrence and thus earn consideration in climatic models.

2.5. Snow Microwave Emissions

The sensitivity of snow brightness temperature to wetness is relatively well understood (Ulaby, 1987) given the high sensitivity of microwaves to changes in surface dielectric properties. Hence, it represents a great potential as a tool in observing and detecting ROS events from space, but detailed information at the ground level is necessary to interpret radiometric response of passive microwave emissions to ROS.

According to Planck's law, all physical matter radiates energy when its temperature is above the absolute zero. This electromagnetic radiation is caused by the kinetic energy produced by the collision of particles within a specific matter, and is directly proportional to its temperature. In the microwave wavelengths, Rayleigh-Jean's approximation defines the intensity of the emitted radiation per unit area. It is then with this specific intensity (I_p), and the direction (elevation angle (θ) and the azimuthal angle (ϕ)), that we can determine the temperature brightness (T_b) of a microwave emission signal.

$$I_p = \frac{KT}{\lambda^2} \quad \text{[eq. 2]}$$

$$T_{bP}(\theta\phi) = I_P\,(\theta\phi)\,\frac{\lambda^2}{K} \quad \text{[eq. 3]}$$

I = Rayleigh-Jean's approximation

K = Stephan-Boltzmann's constant

T = Temperature in Kelvin

θ = Elevation angle

ϕ = Azimuth Angle

By replacing I_p in [eq. 3] by $\frac{KT}{\lambda^2}$ from [eq. 2] and adding an emissivity factor (ε), the brightness temperature equation becomes [eq. 4], where the brightness temperature is a function of emissivity and physical temperature.

$$T_{bP}(\theta\phi) = \varepsilon T \quad \text{[eq. 4]}$$

From snow perspective, a vertical profile is composed of numerous layers, each of which has its own characteristics, such as density, temperature and grain size, that govern the microwave emissions through the dielectric properties. It would be outside of the scope of this paper to go into any great details about the scattering processes and modeling responsible for the acquiring of the T_b. That being said, there is one more important factor that needs to be taken into consideration; the dielectric constant. The

dielectric constant measures the response of a material to an applied electric field. There are three distinct factors that need to be taken into consideration when measuring this response; the temperature, the frequency and the water. The dielectric constant of water, snow and ice are so fundamentally different, that even a small amount of water on the snow surface will have a significant impact on the microwave signal.

3.0. Data and methods

3.1. Study site and period

The "Site Interdisciplinaire de Recherche en Environnement Extérieur" (SIRENE) research station is located on Mont-Bellevue, Sherbrooke. Mont-Bellevue is a relatively a small mountain with its peak at approximately 360 meters above the sea level. The station is located on its south western flank surrounded by deciduous/mixed forest environment. The station's geographic coordinates are N45.373845, W71.923097 (Figure 1)

Meteorological data was measured continuously throughout the winter period of 2012-2013. We will focus the analysis between January 15th and February 7th, where both a warm front and ROS event occurred. At the beginning of the focused period, snow depth was 53mm and during the course of data gathering a complete melt of snow cover occurred on the January 31st. This was mainly due to a raise in temperatures associated with ROS events that happened during that period. In summary, as described in Table 1, the events analyzed in this research spawn over two time periods; January 19th to 20th and January 30th, each period corresponding to a melt and ROS event, respectively. Table 1 also outlines the mean air temperature, the precipitation type and the total amount of precipitation, in its liquid equivalent, measured during the two time periods.

Table 1: The ROS and melt events and their meteorological summary.

Date	Event	Mean air temperature (ºC)	Precipitation	
			Type	Amount (mm)
Jan 19-20th	Melt	1.01	Mainly snow	13.25
Jan 30th	ROS	5.06	Mainly rain	21.9

For the town of Sherbrooke, Weather Canada shows the mean monthly maximum temperatures at -3.5ºC and -3.4ºC for January and February respectively, -15.0ºC and -12.3ºC for the mean monthly minimum temperatures and -9.2ºC and -8.0ºC for the mean monthly average temperatures. Even if the Weather Canada provides the daily precipitation averages for the town of Sherbrooke, their webpage sadly does not make a distinction between the precipitation types: thus making it impossible to identify the ROS events.

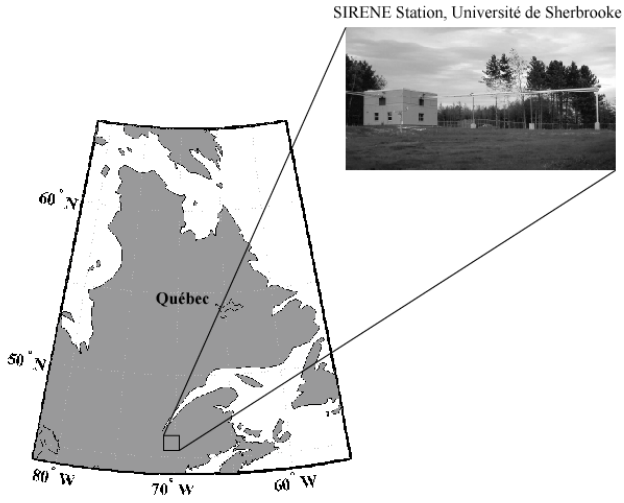

Figure 1: SIRENE research station located in Sherbrooke, Québec, Canada (Langlois et al., 2009).

3.2. On site measurements

3.2.1. Meteorological / remote sensing instruments and measurements

SIRENE is outfitted with the most cutting edge technology in the fields of meteorology and remote sensing. The instruments include; LI-COR LI200SZ, Kipp & Zonen CG1, RM Young 05103-10, Campbell Scientific CS500, Everest 4000.3, CIMEL and Vaisala PWD12.

The LI200SZ is a pyranometer measuring the incoming and reflected solar radiation with a precision of +/- 5% and it can operate in temperatures ranging from -40 to 65ºC. The CG1, a pyrgeometer, measured the longwave radiation emitted by the surface and

it can operate in temperature ranges of -40 to 80ºC with an accuracy of +/- 10%. The 05103-10 is a wind monitor, capable of measuring the wind speed and direction with an accuracy of +/- 0.3 m/s while the ambient temperature and relative humidity was measured with the CS500, with an accuracy of +/- 3%. The Everest 4000.3, an infrared sensor with an accuracy of +/- 0.5ºC, was used to measure the surface skin temperature. The CS705, a tipping bucked rain gauge with a funnel extension, and PWD12 were used to measure the precipitation amounts and the precipitation phase, respectively. The PWD12 is a visibility sensor with a temperature operating range between -40 to 60ºC; it is capable of identifying all 4 types of precipitation using 39 different denominations that were grouped into 3 categories, liquid, mixed, and solid. Snow depth was provided by an ultrasound sensor with a vertical resolution of 1mm and operating temperature range between -40 to 60ºC.

3.2.2. Surface-based radiometer

Two distinct radiometers, designed to emulate the Advanced Microwave Scanning Radiometer (AMSR-E), used onboard the Aqua satellite, were used to collect the 18.7 and 36.5 GHz wavelengths data, in both horizontal and vertical polarizations. During the data gathering period, the field of view of the radiometers was calculated to be 2 X 2 meters. Both radiometers were calibrated simultaneously, before the data gathering period and after, using the ambient temperature microwave absorber (warm) and liquid nitrogen (cold) targets; the uncertainty was estimated at ±2 degrees Kelvin.

4.0. Results

4.1. Overview

As mentioned earlier, the data for this essay was collected between the dates of January 15th and February 7th. As we can see from Figure 2, the snow depth at the beginning of the data collection process was approximately 53mm. Between the 15th and 20th of January the snow thickness rose to approximately 130 mm where it more or less stayed stable until the evening of January 30th where a complete melt of the snow cover occurred over the course of few hours under a ROS event. As we can see from Figure 2, from January 31st to February 6th no snow cover was able to take hold, and only a small amount of snow accumulation occurred on February 6th.

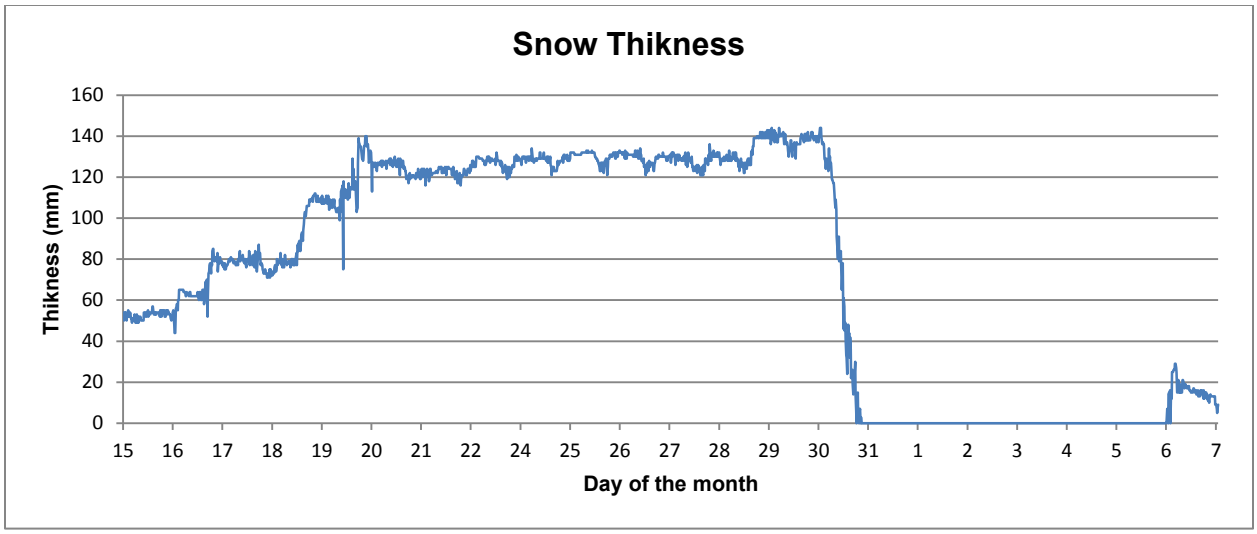

Figure 2: Temporal evolution of the snow thickness (January 15th - February 7th).

As we can see from Figure 3, the air and surface temperatures varied greatly through the data gathering period. In general, both the air and surface were in the sub-zero temperatures. On few occasions, 16th, 17th, 19th, 30th and 31st of January, as well as on the 1st and 3rd of February, temperatures rose above zero. The most significant increases in temperature occurred on the 30th of January through the early hours of 1st of February, where air temperatures rose close to 10°C. As it could have been expected, inversions in the air and surface temperatures happened where the surface temperatures were lower than the air temperatures during the night periods, and the air temperatures were lower than the surface temperatures during the day periods. The incoming solar radiation has a big influence on this inversion cycle; the lower specific heat of snow and naked solid compared to air will absorb more of the incoming solar radiation during the day and thus the surface temperatures will be higher than the air temperature. During the night period, in the absence of incoming solar radiation, the surface will be losing this heat and transferring it to the ambient air in the form of latent heat and longwave radiation, which results in higher air temperatures compared to the surface temperatures (radiative cooling).

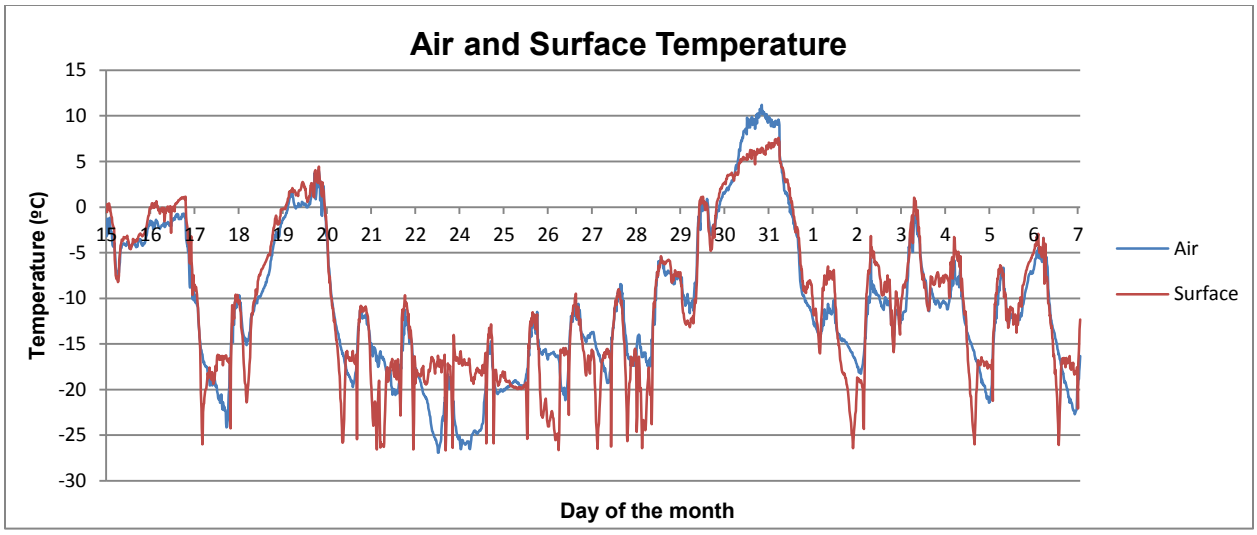

Figure 3: Temporal evolution of the air and surface temperatures.

The air pressure and wind speed measurements also reflect theoretical expectations. The atmospheric pressure varied based on the movements of air masses. Hotter air masses had a relatively lower air pressure in comparison to cooler air masses. The flow air (i.e. wind) happened along those pressure gradients where the wind is strong along steep air pressure gradient and weaker along the less steep pressure gradients. As we can see from Figure 4, two low pressure systems, associated with a warm front, moved in on the 19th-20th and 30th of January. A relatively big difference in the two pressure systems resulted in higher wind speeds as the dense air from the cooler air mass moved toward the less dense warmer air mass in order to create equilibrium. This movement of warmer and cooler air masses is also reflected in Figure 3, where we can clearly see an increase of air temperatures on the 20th (no ROS associated) and 30st of January (associated with ROS), as the warmer air masses were moving in.

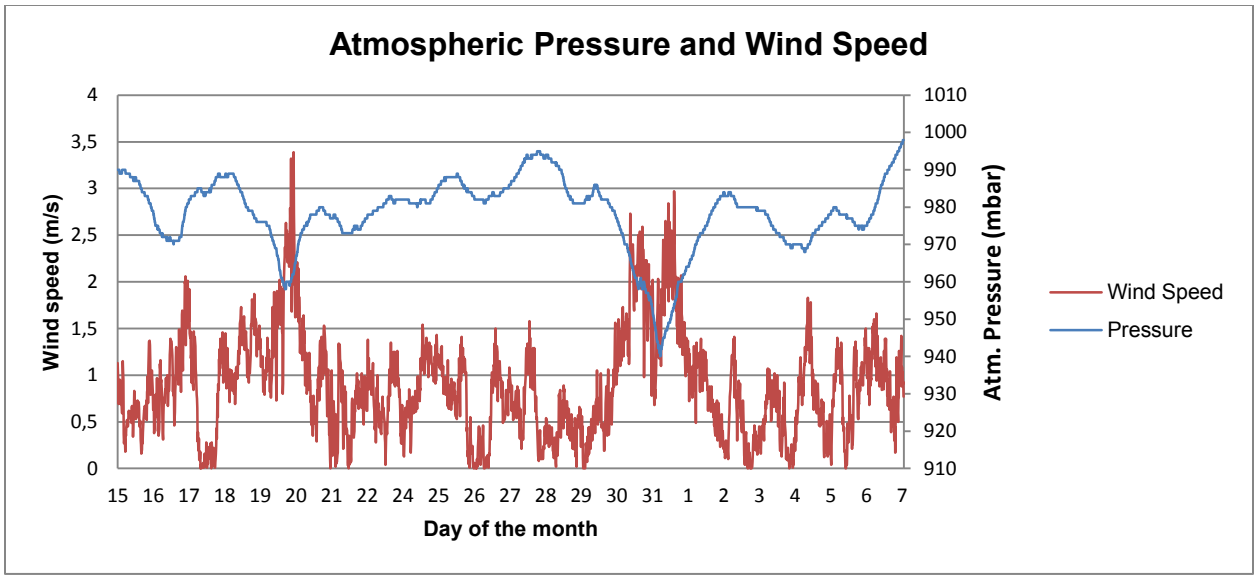

Figure 4: Temporal evolution of the atmospheric pressure and wind speed.

As we can see from Figure 5, the increase in precipitations, on January 30st, coincides with the movement of the high and low pressure systems. As the relatively low pressure system moves in, the movement of air from hotter to cooler air mass, as well as the movement of the relatively hotter air mass over a cooler one will lead to precipitation. Precipitations will take form of snow or rain depending on the meteorological conditions, as explained. The snow precipitation generally results in a growth of snow thickness while the ROS event mostly resulted in a reduction of snow thickness through extensive melt. The resulting liquid water in the snow pack will inevitably have a strong impact on brightness temperature. Furthermore, liquid water possesses a higher thermal conductivity in comparison to air facilitating heat propagation and melt rate. As we can see in Figure 2 and Figure 5, the ROS event that happened on the 30st of January was substantial enough to lead to a complete melt of the snow cover that happened in less than 24h.

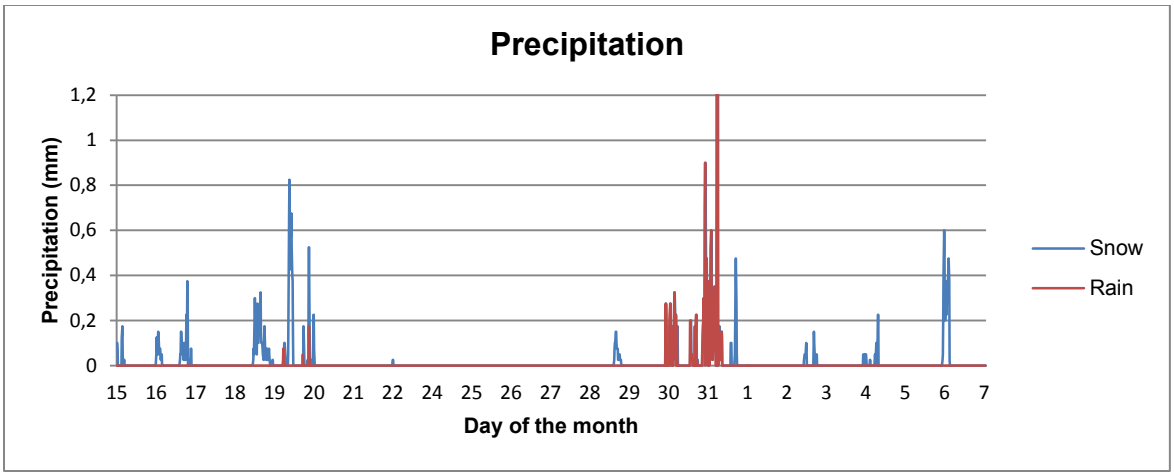

Figure 5: Temporal evolution of the snow and rain precipitations.

4.2. Albedo

In order to produce relevant albedo data, we selected only data that was taken within day time cycles, 8:00AM to 4:00PM. The data was also filtered to eliminate erroneous data given potential data gathering errors caused by environmental conditions and/or the data gathering instrument. Some albedo values appeared unrealistic (higher than 1 or lower then 0); those values were filtered out and may result in albedo values that deviate from the reality. However, the albedo values from Figure 6 and their daily averages found in Table 2 are to a certain degree indicative of snow precipitation and ROS events impacts.

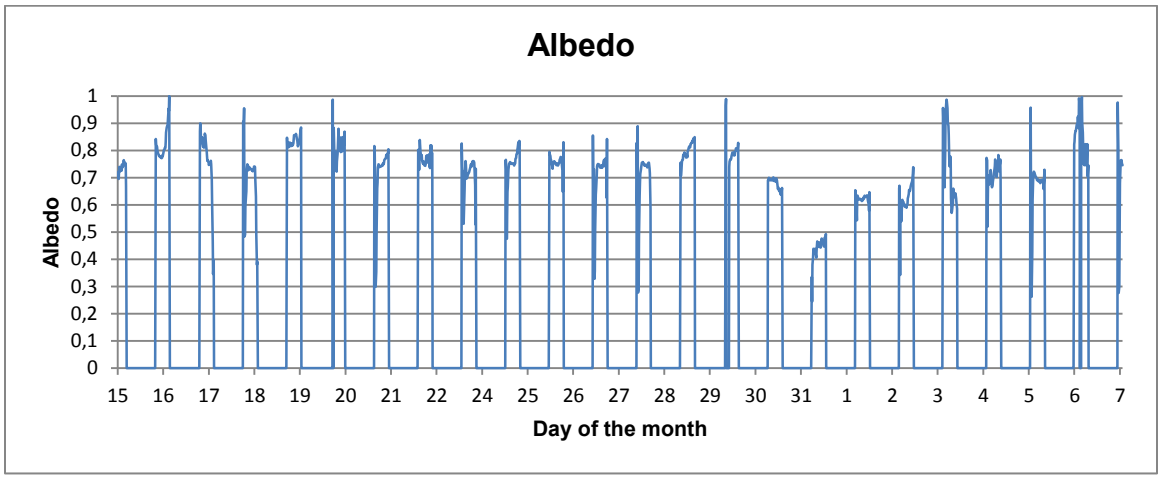

Figure 6: Temporal evolution of albedo.

Fresh snow has a higher albedo value then older snow (Li et al., 2006). This phenomenon is mainly due to the fact that a newly fallen snow crystal still did not have enough time to be dramatically influenced by the compaction and wind, and thus still has a high surface-to-volume ratio (i.e. snow specific surface area, SSA). As such, low density snow will have a higher albedo then a more compacted snow (rounded grains with lower SSA). As we can see from Figure 5 and Figure 2, the most frequent and substantial amounts of snow precipitation happened between January 15th and 20th which is reflected by the snow thickness increasing from 53 mm to approximately 130 mm. Table 2 and Figure 6, clearly show that albedo values were highest during snow precipitation period, ranging above 0.8. The subsequent time period, 21st to 29th of January, was characterised by the absence of precipitation combined with steady snow thickness values. During that particular time period, the wind compaction and destructive metamorphism processes lead to smaller grains with low SSA values leading to a decrease in albedo. This situation is depicted in Table 2, between January 21st and 29th where the albedo ranged between 0.7 and 0.8, clearly reflecting the expected lower albedo values for old snow.

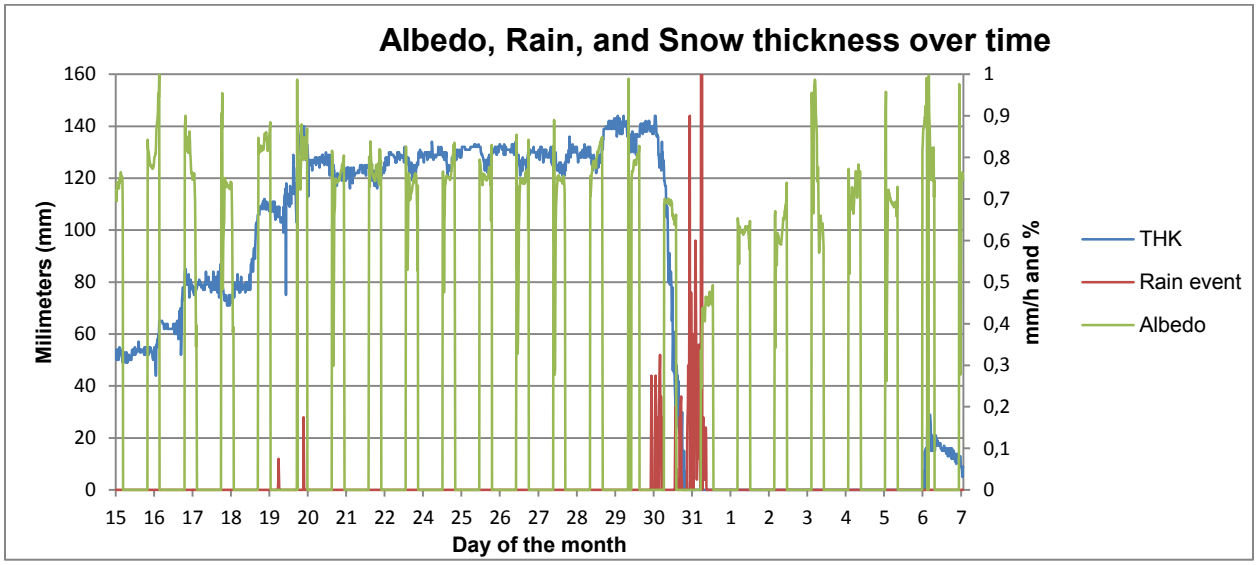

Figure 7: Combined temporal evolution of albedo, rain precipitation, and snow thickness.

Table 2: Daily albedo average evolution (yellow and red outlined data corresponds to melt and ROS events respectively).

Day of the month	Average Albedo	Day of the month	Average Albedo
Jan 15	0,735	Jan 27	0,698
Jan 16	0,827	Jan 28	0,797
Jan 17	0,757	Jan 29	0,788
Jan 18	0,691	Jan 30	0,680
Jan 19	0,837	Jan 31	0,438
Jan 20	0,814	Feb 1	0,621
Jan 21	0,717	Feb 2	0,623
Jan 22	0,773	Feb 3	0,756
Jan 23	0,711	Feb 4	0,714
Jan 24	0,752	Feb 5	0,675
Jan 25	0,757	Feb 6	0,799
Jan 26	0,703	Feb 7	0,665

As we can see from the Figure 7, the melt event on the 20th of January (outlined in yellow on Table 2) resulted in a small reduction in snow thickness, but has not impacted the albedo daily average in any significant way in comparison to other non-ROS day events. This is attributed to the fact that the melt event on the 20th of January was also immediately followed by snow precipitation events. This subsequent fresh snow cover might have masked the wet snow effects on the albedo daily average thus preventing us to make any definitive conclusions simply because the short wave radiation does not have high depth penetration. On the other hand, the ROS event that happened on the 30th of January (outlined in red in Table 2) was important enough to decrease the albedo values. The ROS, as well at the ambient temperatures, resulted in substantial amounts of water present on the surface of the snow cover. Since water has a very low albedo value, ranging between 0.06 and 0.4 depending on the angle of incidence (Cogley, 1979), we can clearly see that the values registered in Figures 6 and 7 as well as in Table 2 are lowest albedo values, with snow as the surface cover type, registered for the entire study period (0.680 daily average). Similar studies have shown wet snow albedo ranging anywhere between 0.4 and 0.75 (Robinson and Kukla, 1984; Barry, 1996)

4.3. Passive microwave response

Before continuing, it is important to understand the difference between the signal depth origins for both 19 and 37 GHz frequencies and their respective horizontal and vertical polarizations. As depicted in Figure 8, vertical polarization has a higher penetration depth then the horizontal polarization; while the 19 GHz frequency has a higher penetration depth than the 37 GHz. Thus, the signal origins for each frequency and their respective polarization will not originate from the same depth from within the snow pack.

Thus under normal (no melt, no ROS) and meteorologically stable circumstances, we can imagine that the T_b for each one of those frequencies will be distributed as depicted in [eq. 5] and represented in Figure 8. The 19 GHz vertical polarizations will have the most penetration potential, and thus will originate from within the deepest and warmest parts of the snow profile.

$$\text{Tb } 19\ GHz\ V > \text{ Tb } 19\ GHz\ H \quad and \quad \text{Tb } 37\ GHz\ V > \text{Tb } 37\ GHz\ H \qquad \text{[eq. 5]}$$

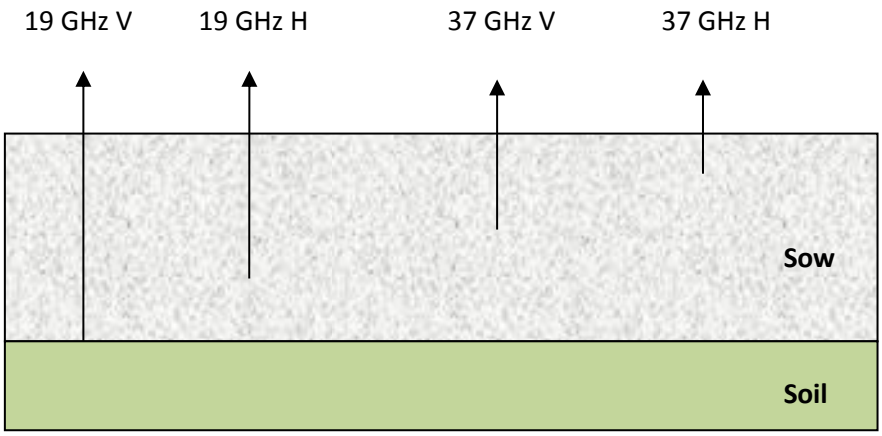

Figure 8: Schematic signal origins for the 19 GHz and 37 GHz frequencies in both of their horizontal and vertical polarizations.

As previously mentioned, the in-situ passive microwave data T_b was collected using surface-based radiometer at 19 and 37 GHz, in both vertical and horizontal polarizations. Both frequencies are also found onboard the AMSR-E satellite (used in this study, but no longer available), which will be used as validation data. As we can see from Figures 9 and 10, the T_b varies greatly with time. In both frequencies and both polarizations, the T_b response will vary depending on the environmental conditions and the properties of the snow pack. The thickness of the snow pack will have an important influence of the microwave signal; the general rule is that the T_b will decrease with an increase of snow pack thickness given the increased volume scattering, until a threshold is reached. The threshold is such that the emission from the ground is completely masked by volume scattering, at which point the T_b will then start increasing given the shorter scattering path. The exact value of that threshold is debated in

different researches (Markus et al., 2006; Derksen et al., 2010; Langlois et al., 2012), the general consensus is that the inversion happens somewhere between 100 and 150mm of snow water equivalent (SWE). The inversion was not seen in our study given the rather shallow snow cover.

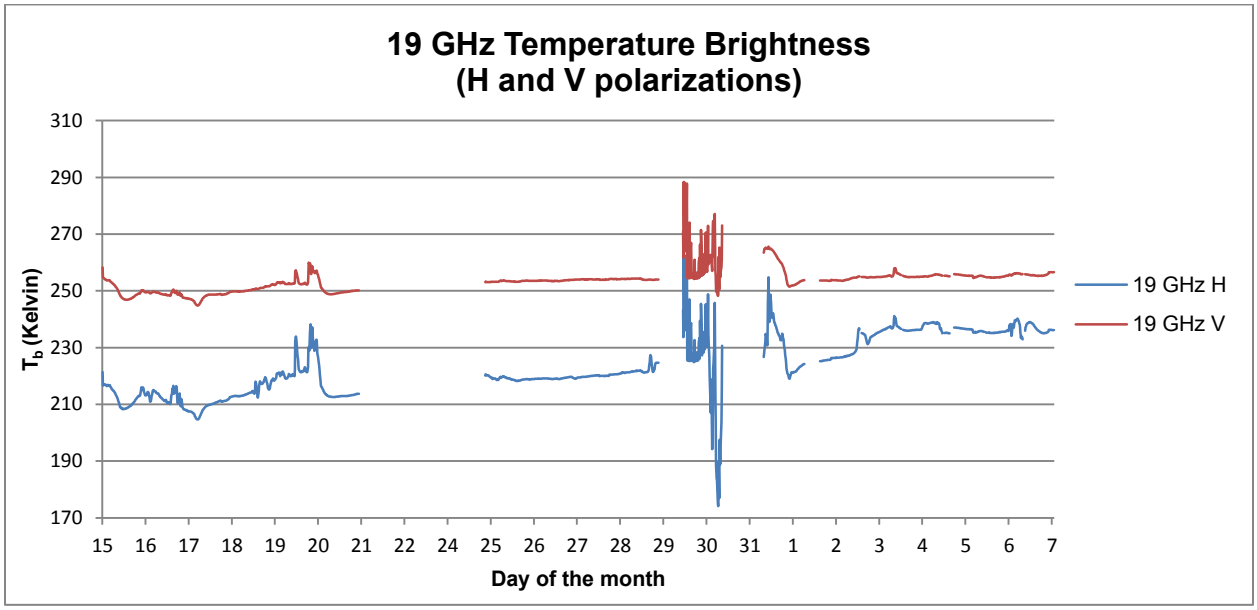

Figure 9: Temporal evolution of the passive microwave brightness temperature for the vertical and horizontal polarizations at 19 GHz.

As previously mentioned, the presence of water in the snow-pack greatly influenced the T_b emissions. The two main examples of that phenomenon happened on the January 19th - 20th and throughout January 30th. In both instances, temperatures rose above 0°C and ROS events occurred only on January 30th. On both dates, in both frequencies and their polarizations, the T_b increased significantly, the highest variation happening on January 30th. The difference between the T_b amplitudes between the two dates is mainly due to substantially higher volumes of water present within the snow pack on January 30th from a more important ROS. It is important to note that the amplitude of the T_b variation differs between the two frequencies and their polarizations. In snow, microwave penetration depth decreases with increasing frequency, thus the emission from deeper are capable of reaching the surface and thus contributing to T_b. As previously mentioned, because of the higher dielectric constant of water, the T_b is more

responsive in 37 GHz wavelength simply because its capable of detecting the cumulative effects of water throughout the snow pack as it propagates through percolation (i.e. more sensitive to water liquid content). Furthermore, according to Fresnel conditions, the emissivity of pure water increases with frequency, and about 5% in emissivity difference can be expected between 19 and 37 GHz frequencies. As show in Figure 10, the resulted emissivity of wet snow increases with frequency. The refreezing of the snow that happened before the complete melt, lead to a sharp decrease in T_b at both frequencies and polarizations through a sharp decrease in the surface emissivity (approximately 30-40%). This decrease has a significant impact considering [eq.4].

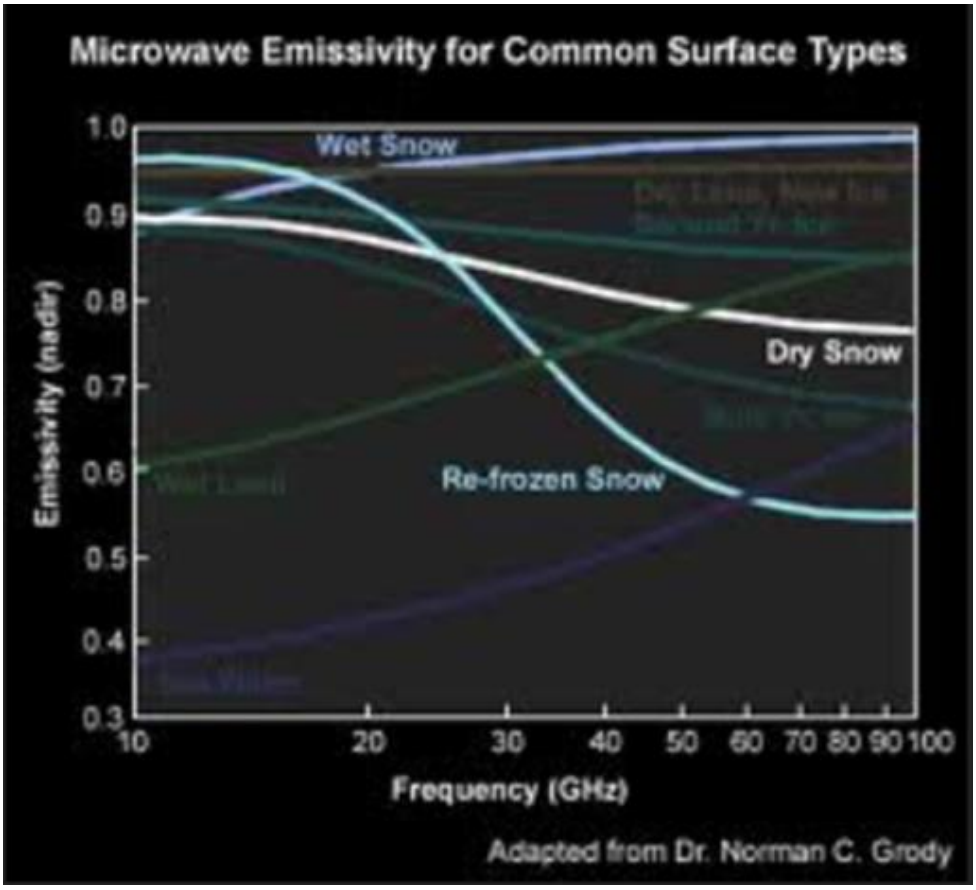

Figure 10: Microwave Emissivity for Common Surface Types (Grody, N.C., retrieved from http://www.meted.ucar.edu).

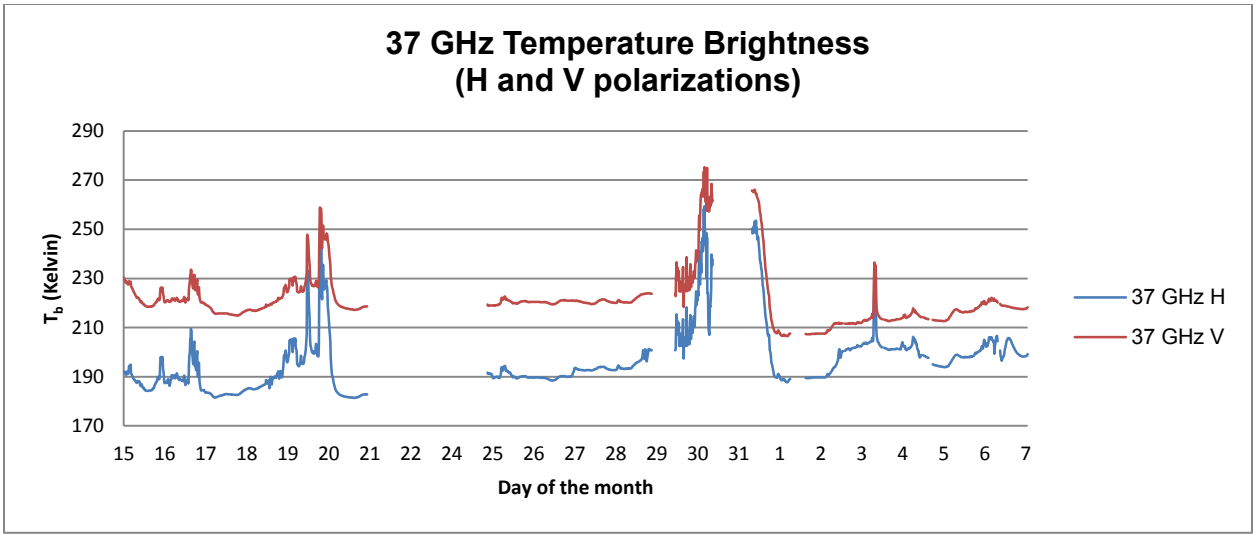

Figure 11: Temporal evolution of the passive microwave brightness temperature for the vertical and horizontal polarizations at 37 GHz.

4.4. Gradient Ratio

Up to this point, we have discussed the meteorological observations and their effects on the passive microwave emission signal. We have clearly seen that the presence of water within the snow pack will greatly influence the T_b measurements. But, we have also seen that the effects of the ambient and surface temperatures, as well as the effects of the snow thickness and metamorphism, will also influence the T_b signal in similar way.

Earlier studies have shown that the gradient ratio (GR) can be used to distinguish between dry and wet snow (Grenfell and Putkonen, 2008). In our study, we have analyzed the melt and ROS events that occurred on the January 19th - 20th and January 30th, respectively. As shown in Table 3, as well as Figures 9 and 11, the T_b values have increased during the ROS event, due to effects of water within the snow column, in all frequencies and polarizations except 19H. The soil contribution to the 19H frequency gets blocked by the water present near the surface of the snow pack. The 19H T_b is assumed to originate from below the surface where the emissivity is lower compared to the 37H due to dryer snow and its lower frequency (see Figure 10). The 37H T_b mostly originates from the wetter/warm and wet surface saturated by water because of its

higher emissivity caused by wetter snow and higher frequency (see Figure 10). This will lead to the T_b of 37H to surpass the 19H. This effect is not observed in the vertical polarization, suggesting that the soil contribution at 19V remains present during our ROS.

In order to be able to better differentiate between the effects of precipitation on T_b, and minimize the effects that the temperature might have on the signal, we need to produce a gradient ratio for the 19 and 37 GHz frequencies, using both of their polarizations. The gradient ratio for two particular wave lengths can be expressed as described in [eq. 6], where GRP represents the gradient ratio for a particular polarisation and T_b is the temperature brightness signal in 19 and 37 GHz wavelength in a specific polarization.

$$GRP = \frac{(T_b\,(p,37Ghz) - T_b(p,19Ghz))}{(T_b\,(p,37Ghz) + T_b(p,19Ghz))} \qquad \text{[eq. 6]}$$

Table 3: Brightness temperature, as well as the GRV, GRH and GRV/GRH ratio avrages for the melt event, ROS events and no event for the 19 GHz and 37 GHz frequencies in both of their horizontal and vertical polarizations.

		Event average		
		Melt	ROS	No event
		Jan 19-20	Jan-30	Jan 26-27
19 GHz	Vertical	255.76	263.63	255.12
	Horizontal	224.81	222.08	220.64
37 Ghz	Vertical	233.79	252.73	221.62
	Horizontal	208.40	228.54	192.16
GRV		-0.05	-0.02	-0.07
GRH		-0.04	0.02	-0.07
GRV/GRH		1.60	0.59	1.03

As mentioned in the previous paragraph, during the ROS event, we have observed the following:

- T_b 19V > T_b 37V: This will lead to a negative, or at least a very low, value of GRV during ROS (depicted in Table 3 as -0.02)

- T_b 19H < T_b 37H: This will lead to a positive GRH value during ROS (depicted in Table 3 at 0.02)

In normal conditions, 19 GHz is expected to be warmer than 37 GHz (at both polarizations) leading to negative values of GR such as observed during our melt event from January 19-20th. Given the fact that 37H > 19H during a ROS event, we propose a new approach using the gradient ratio as described in [eq.7].

$$GRR = \frac{GRV}{GRH} \quad \text{[eq.7]}$$

Once we take into consideration the behaviour of the 19H and 37H frequencies, as described above, and apply them into the new GRR ratio [eq.7] we can expect that the algorithm will take one of the two following forms:

- In normal conditions (no-ROS): 19V > 37V and 19H > 37H so that:
  - GRV = (37V - 19V) / (37V + 19V), GRV = (- / +) = - values of GRV
  - GRH = (37H – 19H) / (37H + 19H), GRH = (- / +) = - values of GRH
- During ROS events, 19V > 37V but 19H < 37H so that:
  - GRV = (37V - 19V) / (37V + 19V), GRV = (- / +) = - values of GRV
  - GRH = (37H – 19H) / (37H + 19H), GRH = (+ / +) = + values of GRH

Therefore, we investigated the ratio of both GRV and GRH (GRV/GRH). Negative GRV/GRH values are expected during ROS events and positive values during normal conditions. The use of GRV/GRH, rather than simply using the GRH, decreases noise in the temporal analysis such as presented in Figure 12 below, where the threshold of 1 seems to be a good separator between ROS and no-ROS events.

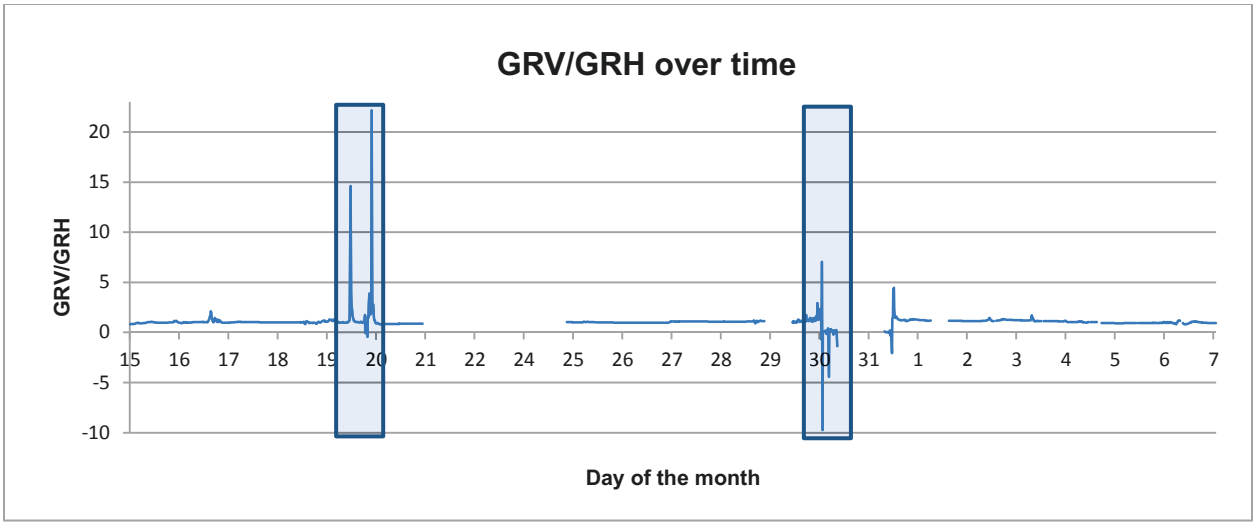

Figure 12: Temporal evolution of the GRV/GRH ratio.

It is only now that we can understand better the importance of the previously stated fact that the ROS event result in the reduction of the T_b values for the 19 GHz H frequency. Under normal circumstances, as the [eq. 5] demonstrates, the T_b for 37 GHz frequencies will always be inferior to the T_b of the 19 GHz V frequencies and that for both of their horizontal and vertical polarizations. However, more work is required to completely understand the complexity behind the relationship between polarizations, emissivity and frequency during melt and ROS events, such as the sharp increase during the melt event. Nonetheless, the behaviour highlighted in Figure 12 is clear and suggest a very distinctive pattern between the normal, the melt and the ROS events. The rate at which the snow cover is being saturated between a melt and ROS events are very different and could explain the different behaviour showed above, but further work measuring wetness in real-time, combined with coincident measurements, brightness temperature and precipitation phase is required.

5.0. ROS detection algorithm

Based on the results obtained in the previous section of this essay, we can begin to formulate an index for detecting the ROS events using passive microwave radiometry (Figure 13). The reasoning behind the classification parameters has been outlined throughout the past sections of this essay, and they have been summed up in Table 4.

One would assume, ROS events imply that the surface cover type is snow; considering any other type of surface cover would be outside of the scope of this research, and the index would not work. Moderate Resolution Imaging Spectroradiommeter (MODIS), part of Earth Observing System (EOS) and Aqua satellites, can provide us, on almost uninterrupted and real time basis, snow cover presence for almost the full extent or the Arctic region. Some formatting would need to be done in order to make the MODIS and AMSR-E datasets compatible; ensuring that both raster data sets are projected in the same way as well as that they are of the same resolution. MODIS raster product has a resolution of 500 meter, while the AMSER-E raster product has a resolution of 25 kilometers. Several down-scaling and up-scaling efforts between MODIS and AMSR-E can be found in the literature, but going into any great details about the procedure would be outside of the scope of this essay. Once that is done, the MODIS snow cover products can be used as a mask to extract their spatial equivalent from the AMSR-E raster product. AMSR-E product can then be broken down to its 19 GHz V, 37 GHz V, 19 GHz H, and 37 GHz H, brightness temperature (T_b) components and then plugged in the GRV and GRH algorithms, which then can be used to produce the GRV/GRH spatial product. Based on the results of the GRV/GRH product, we can then apply the classification algorithms found in Table 4.

Table 4: Classification parameters used in the ROS events detection index.

Classification Parameters	
Classification	**GRV/GRH Condition**
No ROS	GRV/GRH) >= 1
ROS event	(GRV/GRH) < 1

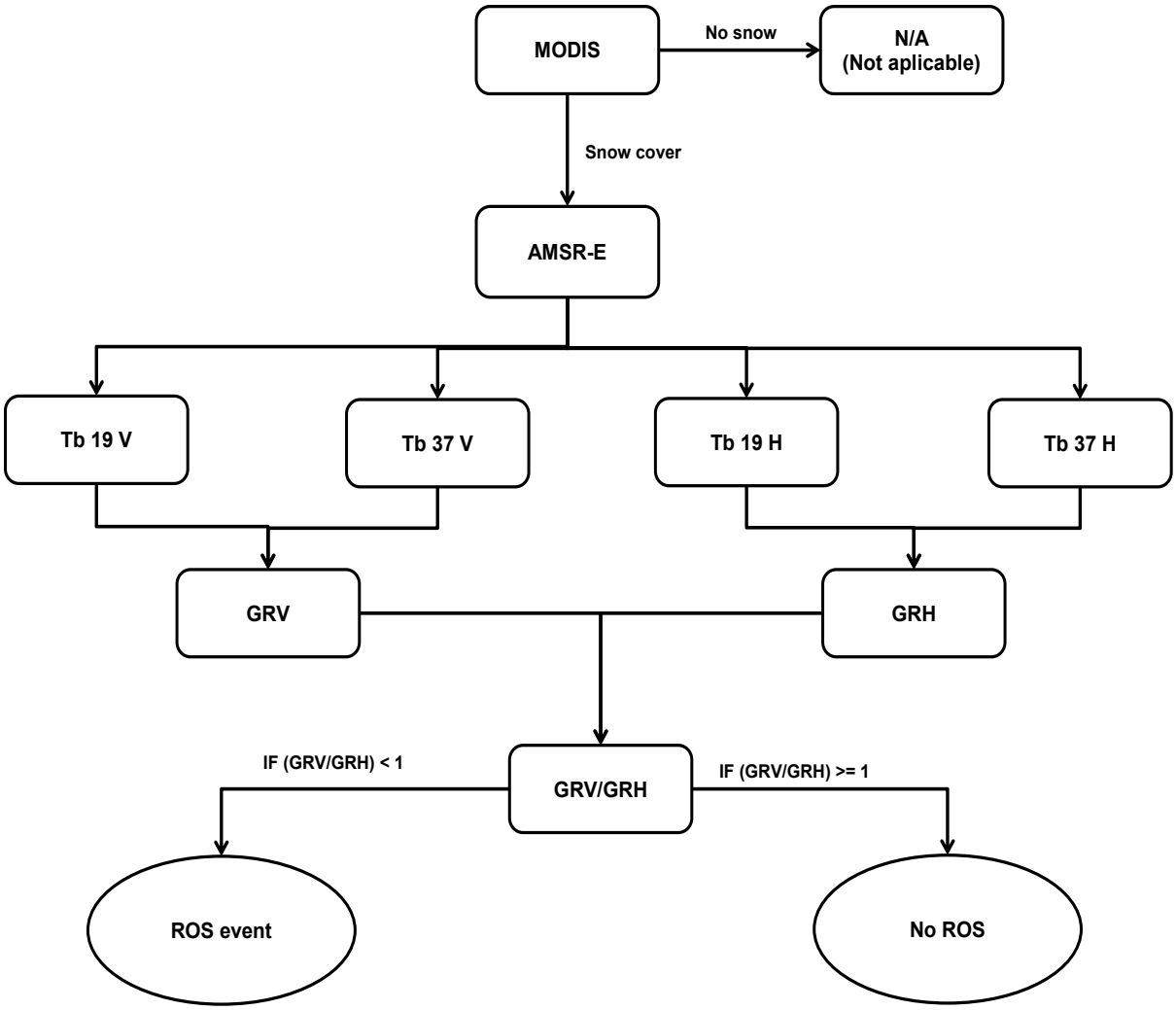

Figure 13: ROS detection index using the GRV/GRH approach.

6.0. Validation of the approach

Environment Canada possesses a wide network of meteorological stations throughout the Canadian national territory. Like previously mentioned, those stations might have some inherent spatial distribution bias, mainly due to economic factors, but data obtained is valid, readily availed, and useful in many situations. In order to test the validity of the ROS detection index developed in this essay the data from the Environment Canada was used. Three meteorological stations, located at the proximity of Inuit communities on the Ungava peninsula, Salluit, Kangiqsujuaq, and Kangirskuk, were selected (Figure 14). The three meteorological stations are at the proximity of the

selected AMSR-E pixels 1, 2 and 3 and all three stations are also supported by human observation data. The three AMSR-E pixel products were selected based on their proximity of the Environment Canada meteorological stations, but also for their inland spatial distribution and relative surface type homogeneity without vegetation and low topography. In Figure 14, the AMSR-E pixels are centered on their real location, which is far from the coast, but their scale has been exaggerated for the purpose of display. The validation data was collected from November 1st 2010 to May 15th 2011, which has been known to be an abnormally warm winter (i.e. increasing the chances of ROS events). Human observations ensured that the snow cover was complete throughout the validation collection period.

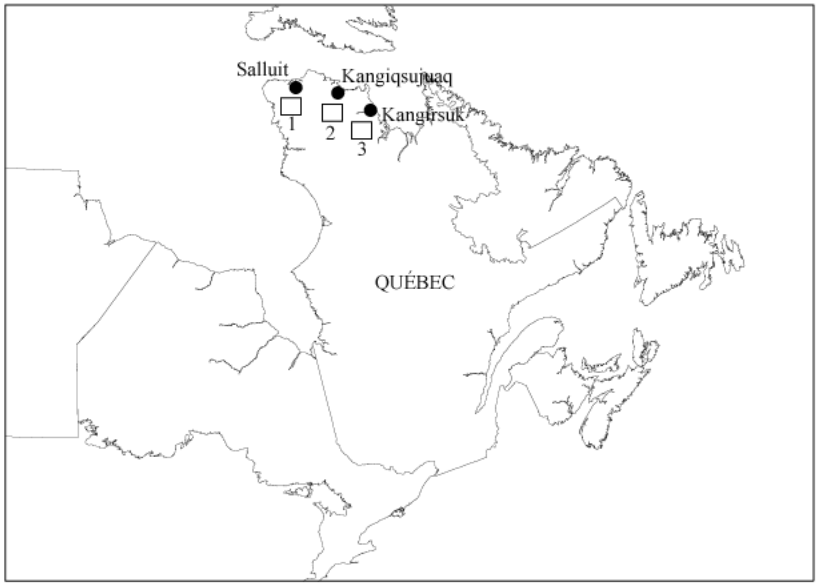

Figure 14: Location of Salluit, Kangisqujuaq, and Kangirskuk Inuit communities and their corresponding AMSR-E pixels.

Human observation played an important part in identifying ROS events throughout the validation data collection period. All of the ROS events observed by monitors throughout the data gathering period are summed up in Table 5 which outlines the location, the date, the air temperature and the hourly duration of the ROS event. ROS events were defined by the human observers as events where a snow cover is present on the

ground during a rain precipitation event. The only limitation of the human observation was that it was made between 8:00 AM and 17:00 PM time periods.

Table 5: ROS event observed by monitors between November 1st 2010 and May 15th 2011, for the selected AMSR-E pixels 1, 2 and 3.

Station	Dates	Tair (°C)	Time rain (local)
Salluit Pixel 1	Nov. 1 2010	0	15:00-16:00
	Nov. 2 2010	-1	11:00-12:00
	Nov. 3 2010	+1.1	07:00-15:00
	Nov. 12 2010	0	08:00-12:00
	Dec. 2 2010	+1.1	15:00-17:00
	Dec. 15 2010	-1.4	10:00-17:00
	Dec. 17 2010	+2.5	15:00-16:00
	May 2 2011	+1.2	12:00-15:00
	May 6 2011	+0.5	07:00-13:00
Kangiqsujuaq Pixel 2	Nov. 12 2010	+3.7	13:00-15:00
	Nov. 25 2010*	+0.2	08:00-13:00
	Nov. 27 2010	+0.5	12:00-14:00
	Dec. 17 2010	0	09:00-14:00
	Jan. 5-7 2011*	-1.6	Continuous
	May 2 2011	-2.6	08:00-09:00
Kangirsuk Pixel 3	Nov. 3 2010	-0.1	15:00-16:00
	Nov. 4 2010	+1	07:00-08:00
	Nov. 8 2010	0	08:00-10:00
	Nov. 12 2010	+2.1	14:00-16:00
	Nov. 24 2010	+1.5	14:00-15:00
	Nov. 25 2010*	+0.5	08:00-17:00
	Nov. 26 2010	+0.8	08:00-14:00
	Dec. 1 2010	-0.2	14:00-15:00
	Dec. 6 2010*	-2.1	08:00-17:00
	Dec. 17 2010	+2.3	17:00
	Dec. 19 2010	+1.4	14:00-15:00
	Jan. 5 2011	-0.3	11:00-13:00
	Jan. 7 2011*	-1.2	11:00-17:00
	Jan. 8 2011*	-1.2	08:00-10:00

AMSR-E data were extracted for the entire study period, and the ROS detection index applied using the criteria and the method outlined in the previous sections of this essay (Figure 13, Table 4). Statistical analysis was then conducted (Table 6 and Table 7), in order to determine the accuracy of the index. The statistical analysis took in to consideration the following:

- **Total number of observations**: The total number of AMSR-E data selected, using the Environment Canada meteorological observations, used in the statistical analysis (November 1st 2010 to May 15th 2011)
- **Human observed ROS**: The total number of ROS events witnessed by the human observers at the Environment Canada meteorological station.

- **ROS index observations**: The total number of ROS events detected by the ROS detection index using the AMSR-E data.
- **Detected ROS with AMSR-E**: The ROS events accurately detected by the ROS detection index.
- **Commission**: The number of times that the ROS detection index perceived the occurrence of the ROS event but the meteorological station made no such observation.
- **Omission**: The number of times that the ROS detection index has not perceived the occurrence of the ROS event, but the meteorological station has.
- **No human observation**: The number of times that there is no data from the meteorological station, but the ROS detection index perceives the occurrence of the ROS event.
- **Accuracy**: The accuracy of the ROS detection index following the [eq. 8] algorithm.

$$Accuracy = \frac{Detected\ ROS\ with\ AMSR{-}E}{Human\ observed\ ROS + Comission} \qquad \text{[eq. 8]}$$

- **Maximum possible error**: This parameter, as its name implies, defines the maximum percentage of accuracy in relation to the total number of observations, as described in [eq. 9], assuming all "no human observations" were wrong.

$$Maximum\ posssible\ error = \frac{Omission + Commission + No\ human\ observation}{Total\ number\ of\ observations} \qquad \text{[eq. 9]}$$

Table 6: The statistical analysis of the ROS detection index using the AMSER-E and Environment Canada data.

	Total number of observations	Human observed ROS	ROS index observations	Detected ROS with AMSR-E	Commis-sion	Omission	No human observations	Accuracy	Maximum possible error
Salluit (1)	257	12	18	12	1	0	5	92%	2.3%
Kangiqsujuaq (2)	258	7	24	5	2	2	17	56%	8.1%
Kangirsuk (3)	244	15	34	12	6	3	16	57%	10.2%
All 3 pixels	759	34	76	29	9	5	38	67%	6.9%

Table 7: ROS detection index matrix.

In-situ / AMSR-E	Ros	No ROS	TOTAL
ROS	76	9	85
No ROS	5	669	674
TOTAL	81	678	759

The overall potential of the ROS detection index appears to be satisfactory; 67% accuracy and 6.9% maximum possible error. The Salluit (pixel 1), Kangiqsujuaq (pixel 2), and Kangirsuk (pixel 3) index accuracies are 92%, 56% and 57%, respectively. It is important to note that even if the overall accuracy of the pixel 2 and 3 might appear low, the number of "Detected ROS with AMSR-E" ratio, 5/7 (71%) and 12/15 (80%), is still high and indicative of the index's potential. The low number of omissions for all three pixels, 0, 2 and 3 in their respective order, further reinforces the previous statement showing that the index's classification parameters do not under-reach their objectives in any significant way. This is confirmed even further by the low maximum possible error of 2.3%, 8.1% and 10.2% for the three pixels by taking into account the high amount of AMSR-E passes used in the validation. For the pixels 1 and 2, the low number of commissions, 1 and 2 respectively, further reinforces the index's accuracy potential by indicating that the index does not substantially overreach with its classification parameters. For the pixel 3, the high number of commissions, six in total, might appear misleading; but, it is important to also consider the "Total number of observations" as well as the significance of "No human observations". Even if the "No human observations" statistic does influence the accuracy value, it is still symptomatic of the potential number of "Detected ROS with AMSR-E" that could have been made, indicating that the accuracy value could change if a methodology could be developed to compensate for the "No human observation" values. Finally, if we take into consideration the high variability of the brightness temperatures, the "Total number of observations" made for the validation process, and the ever changing meteorological conditions that influence the snow properties, we can conclude that the ROS detection method shows great potential in detecting ROS events.

7.0. Discussion of limitations

As we have seen, creating a ROS detection index involves understanding and integrating a large quantity of practical and theoretical knowledge from multiple fields of science. Knowledge in remote sensing, meteorology, environmental sciences, as well as basic quantitative methods has been required in order to complete this essay. Never the less, even if the results of the validation process performed in the earlier paragraph appear to be satisfactory, it is important to mention some of the limitations that we have noticed while performing this research.

Previously we have noted the existence of a threshold where the brightness temperature becomes lower as the snow thickness rises because of the increased scattering caused by the rising snow column. Once the threshold of the snow thickness is reached the brightness temperature will start rising with the depth of the snow column. In this research the snow depth was 53 mm at the beginning of the data gathering period, and never rose above 150 mm. Thus, at this time, it has not been verified if the index is also applicable in both of those situations.

As we have seen, the brightness temperature will strongly vary depending on the surface type; the presence of ice, ocean, lakes, vegetation, as well as any other Arctic land cover type, will highly influence the passive microwave temperature brightness signal. Even if the validation process showed promising results with an AMSR-E product, which has a spatial resolution of 25 Km by 25 Km, it is important to note that the spatial heterogeneity could influence the index results. It is also important to note difference in the spatial location of the meteorological station data and the GRV/GRG AMSR-E products used to validate the index. It was feared that the spatial bias intrinsic to the coastal communities would influence the validation of the index. Thus, more spatially homogenous locations were selected at the proximity of each community. It was assumed that the meteorological conditions were the same for both locations even if a substantial spatial disparity is present.

In this research, it was assumed that the ROS event is the only method by which the volume of water will rise within a snow column. It is important to note, that multiple thermodynamic processes could also result in the rise of melt water within the snow

column and that the index could confuse it with a ROS event. For example, extreme rise in temperature levels, as well as compaction, can result in snow melting. As previously mentioned, more work will be needed in order to better understand the complexity behind relationships between polarization, emissivity and frequency during ROS and melt events.

8.0. Conclusion

In conclusion, we have seen that the climate change is occurring on a wide range of temporal and spatial scales in response to various environmental and anthropocentric forcing. The Artic is a highly climate change sensitive part of our planet, where a wide range of positive and negative feedback cycles entwine and result, as well as contribute, to some of the most inconvenient climate change scenarios (i.e. desertification, habitat destruction, global rise of sea levels, intensification of meteorological events…). These results might be inconvenient but they are, if an academically unorthodox quote might be permitted, “An Inconvenient Truth”. Many scientists have recognized and tried to understand this problem from a wide range of different point of views in the last two centuries. To understand the “why?” and the “how?” of the climate change might allow us to understand the root of the problem, predict the implications and mitigate the negative consequences. It is with that type of spirit in mind that we have examined the rain on snow events through a microwave perspective.

The brightness temperature, in both horizontal and vertical polarizations for the 19 GHz and 37 GHz is highly dependent on the properties of snow and the ambient meteorological conditions. Any negative or positive change in the snow column thickness and wetness will result in the respective attenuation or amplification of the components of the passive microwave signal through the dielectric properties. As the snow thickness increases, the T_b signal will decrease until a threshold is reached. Augmenting the ratio of water present within the snow column will result in T_b signal increase for 19 GHz V, 37 GHz V, and 37 GHz H, but will result in a reduction of the 19 GHz H T_b signal because the water will mask the microwave signal coming from the underlying soil usually perceived by the 19 GHz frequency.

We have also seen that the snow wetness will also influence the albedo properties of the snow surface in a negative way. ROS events will inevitably cause an increase of water present within the snow column reducing the snow surface albedo value, inevitably impacting snow's energy balance equation. ROS events can cause greater amounts of incoming shortwave solar radiation to be absorbed by the snow surface, promoting melting, and playing into the positive feedback cycle of the climate warming.

It is by understanding the implications of the previously stated observations that we came to realize that we can create an index, using the GRV/GRH ratio, capable of detecting the occurrence of ROS events. As demonstrated with the validation portion of this essay, the index shows great potential with promising results, while a lot of work on snow thickness and vegetated pixels has to be conducted.

Lastly, this essay only aimed at examining ROS events through a passive microwave perspective. A more in depth research and fine tuning of the proposed index will be needed in order to produce satisfactory results with higher degrees of certainty. Never the less, it is our hope, that this research contributed in some way to the greater understanding of the "why?" and the "how?" of the climate change.

LITERATURE CITED

Arctic Climate Impact Assessment (ACIA), 2004, Impact of a Warming Arctic. *Cambridge University Press*

Arslan, A.N., Wang, H., Pulliainen, J., and Halikainen, M., 2001, Effective permittivity of wet snow using strong fluctuation theory, *Progress in Electromagnetic Research*, 31, pp.279-296

Barry, G.R., 1996, The parameterization of surface albedo for sea ice and its snow cover, *Progress in Physical Geography*, 20, pp.63-79

Brown, R.D., Brasnett, B., and Robinson, D., 2003, Gridded North American monthly snow depth and snow water equivalent for GCM evaluation, *Atmosphere and Ocean*, 41, pp.1-14

Brown, R.D., and Mote, P.W., 2008, The Response of Northern Hemisphere Snow Cover to Changing Climate, *Journal of Climate*, 22, pp.2124-2145

Cogley, J., Grahm, 1979, The Albedo of Water as a Function of Latitude, *Monthly Weather Review*, 107, pp.775-781

Derksen, C., Toose, P., Rees, A., Wang, L., English, M., Walker, A., and Strum, M., 2010, Development of a tundra-specific snow water equivalent retrieval algorithm for satellite passive microwave data, *Remote Sensing of Environment*, 114, pp.1699-1709

Derksen, C., and Brown, R., 2013, Spring snow cover extent reduction in the 2008-2012 period exceeding climate model projections, *Geophysical Research Letters*, doi:10.1029/2012GL053387

Dutra, E., Balsamo, G., Viterbo, P., Miranda, P.M.A., Beljaars, A., Schar, C., and Elder, K., 2010, An imporoved snow scheme for the ECMWF land surface model: Description and offline validation, *Journal of Hydrometeorology*, 11, pp.889-916

Fletcher, C.G., Hardiman, C., Kushner, P.J., and Cohen, J., 2009, The dynamical response to snow cover perturbations in a large ensemble of atmospheric GCM integrations, *Journal of Climate*, 22, pp.1208-1222

Ford, D.J., Smith, B., and Wandel, J., 2006, Vulnerability of climate change in the Arctic: A case study from Arctic Bay, Canada, *Global Environmental Change*, 15, pp.145-160

Francis, J.A., Hunter, E., Key, J.R., and Wang, X., 2005, Clues to variability in Arctic minimum sea-ice extent, *Geophysical Research Letters*, p.4

Grenfell, T.C., and Putkonen, J., 2008, A method for the detection of the severe rain-on-snow event on Banks Island, October 2003, using passive microwave remote sensing, *Water resources research*, 44, pp.1-9

Grody, N.C., *Microwave Emissivity for Common Surface Types*, retrieved from http://meted.ucar.edu

Hardiman, S. C., Kushner, P.J., and Cohen, J., 2008, Investigating the ability of general circulation models to capture the effects of Eurasian snow cover on winter climate, *Journal of Geophysical Research: Atmosphere*, 113, p.9

Intergovernmental Panel on Climate Change (IPCC), 2013, Climate Change 2013 The Physical Science Basis, p.2216

Kattsov, V.M., and Kallen, E., 2005, Future climate change: modeling and scenarios for the Arctic, Arctic Climate Impact Assessment Scientific Report, *Cambridge University Press*, Cambridge, pp.99-150

Kaufman, D.S., Schneider, D.P., McKay, N.P., Ammann, C.M., Bradley, R.S., Briffa, K.R., Miller, G.H., Otto-Bliesner, B.L., Overpeck, J.T., Vinther, B.M., Abbottm M., Axford, Y., Bird, B., Birks, H.J.B., Bjune, A.E., Briner, J., Cook, T., Chipman, M., Francus, P., Gjewski, K., Geirsdottir, A., Hu, F.S., Kutchko, B., Lamoureux, S., Loso, M., MacDonald, G., Peros, M., Porinchu, D., Schiff, C., Seppa, H., and Thomas, E., 2009, Recent warming reverses long-term Arctic cooling, *Science*, 325, pp.1236-1239

Kelly, R., Chang, A.T.C., Tsang, L., and Foster, J., 2003, A prototype AMSR-E global snow area and snow depth algorithm, *IEEE Transactions on Geoscience and Remote Sensing*, 41, pp.230-242

Langlois, A., Brucker, L., Kohn, J., Royer, A., Derksen, C., Cliche, P., Picard, G., Willeemmet, J.M., and Fily, M., 2009, Simulation of Snow Water Equivalent (SWE) Using Thermodynamics Snow Models in Québec, Canada, *American Meteorological Society*, 10, pp.1447-1463

Langlois, A., Royer, A., and Goita, K., 2010, Linkages between simulated and spaceborne passive microwave brightness temperatures with in-situ measurements of snow and vegetation properties, *Canadian IPY Special Issue of Canadian Journal of Remote Sensing*, 36, No.1, pp.135-148

Langlois, A., Royer, A., Dupont, F., Roy, A., Goita, K., and Picard, G., 2011, Improved vegetation corrections for satellite passive microwave remote sensing using airborne radiometer data, *IEEE Transactions on Geoscience and Remote Sensing*, 49, No.10, pp.3824-3837

Langlois, A., Royer, A., Derksen, C., Montpetit, B., Dupont, F., and Goita, K., 2012, Coupling of the snow thermodynamic model SNOWPACK with the Microwave Emission Model for Layered Snowpacks (MEMLS) for subarctic and arctic Sow Water Equivalent retrievals, *Water Resources Research*, 48, W12524, p.14

Langlois, A., Bergeron, J., Brown, R., Royer, A., Harvey, R., Roy, A., Wang, L., and Thériault, N., 2013, Evaluation of CLASS 2.7 and 3.5 simulations of snow cover from the Canadian Climate model (CRCM4) over Qébec, Canada, *Journal of Hydrometeorology*, Submitted April 2013, AMSJHM-S-100073

Li, Z., Goloub, P., Devaux, C., Gu, X., Qiao, Y., and Zhao, F., 2006, Retrival or aerosol optical and physical properties from groundbased spectral, multi-angular and polarized sun-photometer measurements, *Remote Sensing Environment*, 101, pp.519-533

Liston, E.G., and Hiemstra, A.C., 2011, The changing cryosphere: Pan-Arctic snow trends (1979-2009), *Journal of Climate*, 24, No.21, pp.5691-5712

Makynen, M., and Hallikainen, M., 2005, Passive microwave signature observations of the Baltic Sea ice, *International Journal of Remote Sensing*, 26, pp.2081-2106

Markus, T., Powell, D.C., and Wang, J.R., 2006, Sensitivity of passive microwave snow depth retrievals to weather effects and snow evolution, *IEEE Transactions on Geoscience and Remote Sensing*, 44, pp.68-77

Putkonen, J., and Roe, G., 2003, Rain-on-snow events impact soil temperatures and affect ungulate survival, *Geophysical Research Letters*, 30, p.1188

Rahmstorf. S., 2007, A semi-empirical approach to projecting future sea-level rise, *Science*, 315, pp.368-370

Read, P., and Lermit, J., 2005, Bio-energy carbon storage (BECS): A sequential decision approach to the threat of abrupt climate change, *Energy*, 30, pp.2654-2671

Robinson, A., David, and Kukla, George, 1984, Albedo of a Dissipating Snow Cover, *Journal of Climate and Applied Meteorology*, 23, pp.1626-1634

Romanovsky, V.E., Smith, S.L., and Christiansen, H.H., 2010, Permafrost thermal state in the polar Northern Hemispehre during the international polar year 2007-2009: a synthesis, *Permafrost Periglac*, 21, pp.106-116

Roy, A., Royer, A., Wigneron, J.P., Langlois, A., Bergeron, J., and Cliche, P., 2012, A simple parameterization for a boreal forest radiative transfer model at microwave frequencies, *Remote Sensing Environment*, 124, doi:10.1016/j.rse.2012.05.020

Schrank, E.W., 2007, The ACIA, climate change and fisheries, *Marine Policy*, 31, pp.5-18

Steffen, K., and DeMaria, T., 1996, Surface energy fluxes over Arctic winter sea ice in Barrow Strait, *Journal of Applied Meteorology*, 35, pp.2067-2079

Ulaby, F.T., Moore, R.K., and Fung, A.K., 1986, Microwave Remote Sensing. 3, Artech house, Norwood, MA.

Vincent, L.A., and Mekis, E., 2006, Changes in daily and extreme temperature and precipitation indices for Canada over the twentieth century, *Atmosphere-Ocean*, 44, pp.177-193

White, W.C.J., Alley, B.R., Brigham-Grette, J., Fitzpatrick, J.J., Jennings, E.A., Johnses, J.S., Miller, H.G., Narem., R.S. and Polyak, L., 2010, Past rates of climate change in the Arctic, *Quaternary Science Reviews*, 29, pp.1716-1727